Probing indirect exciton complexes in a quantum dot molecule via capacitance-voltage spectroscopy

Shovon Pal,[1,2,*] Clara Junggebauer,[1] Sascha R. Valentin,[1] Pia Eickelmann,[1] Sven Scholz,[1] Arne Ludwig,[1,†] and Andreas D. Wieck[1]

[1]*Lehrstuhl für Angewandte Festkörperphysik, Ruhr-Universität Bochum, D-44780 Bochum, Germany*

[2]*AG Terahertz Spektroskopie und Technologie, Ruhr-Universität Bochum, D-44780 Bochum, Germany*

(Received 4 September 2016; revised manuscript received 29 October 2016; published 27 December 2016)

Capacitance-voltage spectroscopy has proved to be a very powerful experimental technique towards the investigation of carrier-carrier interactions both qualitatively and quantitatively in complex coupled nanostructures. Here, we exploit this method to observe indirect exciton complexes in a quantum dot molecule and to quantify the electron-hole interactions between two dots in a quantum dot molecule, formed by vertical stacking of self-assembled quantum dot layers. While frequency-dependent measurements distinguish between the *s*- and *p*-charging behavior, under perpendicular magnetic fields, reordering of the quantized states charging sequence is observed along with the formation of a Landau fan in the wetting layer that is used to reconstruct the Fermi energy level.

DOI: 10.1103/PhysRevB.94.245311

I. INTRODUCTION

Semiconductor quantum dots (QDs) have provided us a huge playground not only for exploring fundamental physics but also in the realization of challenging goals in modern solid-state physics. With the development of high-quality semiconductor nanostructures in the past few decades, researchers have drawn much attention on the investigation of coupled systems [1–5]. These coupled structures have proved to be the building blocks of many electronic [6] and optoelectronic devices [7–9]. Apart from the application front, interest has also been extended towards the study of coherent manipulation and electrical or optical control of these quantum-mechanically coupled systems. While single QDs have attracted the quantum information processing community [10,11], quantum dot molecules (QDMs) offer a further scalability for implementing two-qubit operation and thus extend the goals for the realization of more complex quantum processors [12–14]. Supporting the above statement, recent experiments have demonstrated a much faster dephasing with increasing quantum mechanical coupling in these structures [15,16]. Moreover, external electric fields can be used as a steering wheel to manipulate carrier localizations [3,17] and excitonic states [18–21] within. Such fields can be easily applied using a suitable gate (Schottky or more recently epitaxial [22]) in a charge-tunable device structure, a prototype of which is investigated in this paper.

A quantum dot molecule [23] is a system of two quantum-mechanically coupled dots in a vertically stacked pair of islands. There are several ways of realizing such structures, of which strain-induced Stranski-Krastanov (S-K) [24] mode is the most common one. The strain that surrounds a dot in the first layer enforces the growth of the second dot on top of it [16,25], although with the S-K growth mode the dots obtained in both the layers are self-assembled ensembles. This leads to a slight variation of the QD sizes in the two layers: the dot in the upper layer being slightly smaller than the bottom owing to strain-induced nucleation [26]. There have been several spectroscopic investigations on such samples that suffer from inhomogeneous broadening [27], which eventually lead to the modification of such structures by introducing S-K growth with In flushing [28–30]. In this paper, we characterize the QDM samples without In flushing in a charge-tunable structure design by capacitance-voltage [C-(V)] spectroscopy [31,32]. While C-(V) spectroscopy on these structures provides valuable information on the Coulomb dominated carrier-carrier interactions [33,34], studies have not been extended to investigate the formation of excitons in QDMs by illumination-induced holes [35]. Our results show the direct observation of indirect excitons in a QDM electrically, where we were able to resolve five charging peaks in the reverse bias direction. We show that these peaks correspond to the charging events into the lowest electron state of one QD layer and a distinct number of holes occupied in the second QD layer.

The paper is organized in the following manner: In Sec. II, we discuss the sample design and characteristics along with the relevant principles governing the capacitance-voltage spectroscopy. In Sec. III, the photoluminescence measurements of two QDM samples are presented and compared with that of the single layer QD sample. An attempt to analyze the formation of coupled states between the two layers of QDs for an ensemble is also discussed via the voltage-dependent photoluminescence measurements both at 300 K and 77 K. Section IV deals with the frequency-dependent C-(V) measurements where the suppression of QD states with higher AC modulation frequency is discussed. In Sec. V, we discuss the reordering of charging sequence and Zeeman splitting along with the observation of a Landau fan in the wetting layer. Finally, in Sec. VI we present the unique features observed in the C-(V) spectra of QDM samples as a result of illumination with a near-infrared light emitting diode (NIR-LED). Conclusions and perspectives are presented in Sec. VII.

II. SAMPLE AND METHOD

The investigated samples are grown on a semi-insulating GaAs (100) substrate using molecular beam epitaxy (MBE).

*Current address: NEST, Istituto Nanoscienze-CNR and Scuola Normale Superiore, Piazza San Silvestro 12, Pisa, I-56127; shovon.pal@ruhr-uni-bochum.de

†arne.ludwig@ruhr-uni-bochum.de

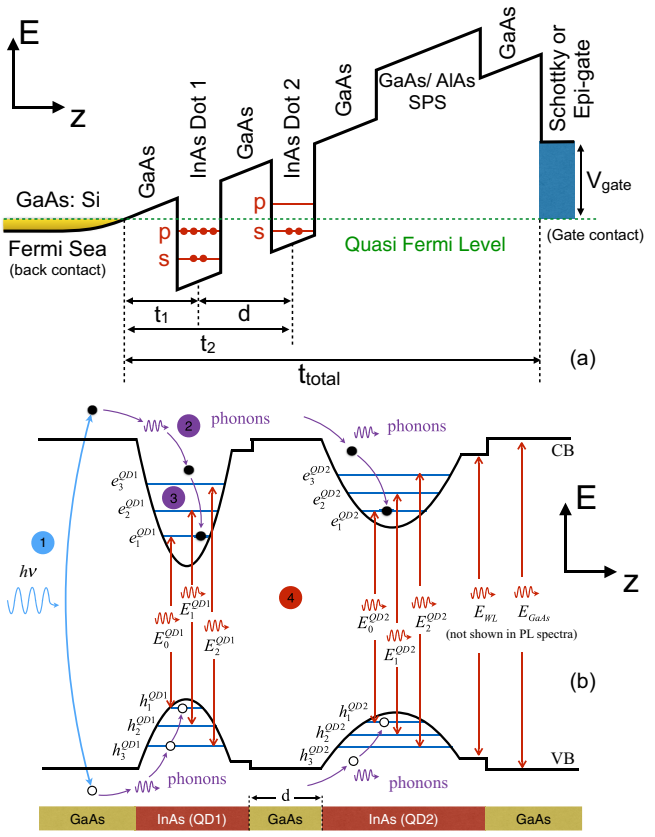

FIG. 1. (a) Schematic of the conduction band edge E_c, of the quantum dot molecule sample, which is designed in a bias tunable structure with bulk-doped n^{++} GaAs layer serving as the back contact and Schottky gate on top. The two QD layers are separated by a distance of d. t_1 and t_2 are the thickness of the tunnel barriers for the first and second dot layer, respectively, while t_{total} is the distance between the Fermi sea (back contact) and the gate contact. (b) Schematic of the transitions observed in the photoluminescence spectroscopy. The processes involved are: 1) Formation of electron-hole pair by laser excitation. 2) Nonradiative relaxation into QD states. 3) Relaxation to ground state. 4) Recombination and emission of photons.

All samples are grown in bias/charge-tunable metal-insulator-semiconductor (MIS) Schottky diode structures with a bulk-doped n^{++} layer behind that serves as the reservoir of electrons and thus as a back contact (BC). Three samples are investigated: *Sample 1*, which has a single layer of InAs self-assembled QDs (SAQDs) separated from the BC by a tunnel barrier of 30 nm. *Sample 2*, which has two InAs SAQD layers spaced 11 nm apart. The tunnel barrier of the first layer is 30 nm and 41 nm for the second layer. *Sample 3* also has two QD layers that are separated by 9 nm. The tunnel barrier of the first layer is 33 nm and that of the second layer is 42 nm. A schematic of the conduction band edge of the QDM sample is shown in Fig. 1(a). The MBE-grown InAs SAQDs are realized by S-K growth mode [24]. The QDs are then capped by a few nanometers of GaAs followed by a blocking barrier that consists of several periods of AlAs/GaAs short-period-superlattice (SPS). The specific growth conditions adopted in this study result in the fact that the QDs in the second layer of the stack are slightly thinner and wider than the QD in the first layer, owing to strain conditions during MBE growth. For the gate contacts, either Schottky or epitaxial gates are used. By definition, an epitaxial gate is a complementary-doped, semitransparent electrostatic gate that can be grown lattice-matched and monolithically on a semiconductor within the ultra high vacuum conditions of MBE. It is composed of a 25 nm thick p^{++}-GaAs layer, followed by roughly 40 periods of carbon-δ-doped and 0.5 nm p^{++}-GaAs layers. The direct semiconductor GaAs allows for a fast (ns) modulation of its electron density also in this *pn*-junction-gate configuration.

In C-(V) spectroscopy, a small AC signal (sine wave) of approximately 10 mV is applied to the gate superimposed on a DC signal that is swept over a voltage range. As the voltage is swept, the charging of different QD levels with electrons are observed as distinct changes in the capacitance between the top gate and the back contact. Based on a simple lever-arm rule [31,32,36,37], the gate voltages can be converted into bias-dependent energies, $E(V_g)$ using:

$$E(V_g) = e\frac{t_i}{t_{\text{total}}}(V_{bi} - V_g), \tag{1}$$

where t_{total} is the distance between the BC and the top gate, t_i is the thickness of the tunnel barrier (with $i = 1,2$), e is the elementary charge, V_{bi} is the built-in voltage (in our samples this is typically 1.03 V), and V_g is the applied gate voltage. In this approach, it is assumed that the interface between the back contact (heavily bulk-doped n^{++} layer) and the tunnel barrier (GaAs) is the pivot for the lever. Besides, the effective dielectric permittivity across all the semiconductor layers is assumed to be a constant. It has been shown that the above assumptions agree very well with the corresponding results from infrared transmission measurements [22,38]. Apparently, the energy spacing of the quantized states and other effects like Coulomb interactions between the electrons within a QD are not affected by the changes in the permittivity introduced by the SPS.

III. OPTICAL INVESTIGATION

The interband transitions between the valence and the conduction bands are characterized by both room temperature and low temperature (77 K) photoluminescence (PL) spectroscopy. A modulated laser diode, which emits at 638 nm (1.94 eV), is used to excite the sample and generate carriers (electrons and holes in conduction and valence band, respectively). These photogenerated carriers relax both nonradiatively via phonons and radiatively via photons. The radiative emissions are dispersed by a spectrometer and then detected by a liquid-nitrogen-cooled InGaAs photodiode. These processes along with the PL transitions are shown schematically in Fig. 1(b). The sample is mounted in a cryostat on a chip carrier that is later used to perform bias-dependent PL measurements. Since several gates (of variable dimensions) are processed on the sample, to locate the correct gate the photovoltage (or photocurrent) is measured when the sample is excited with the laser. The same gate is later used to perform the C-(V) spectroscopy. On shining the laser, a photovoltage of approximately 600 mV is observed between the top gate and the back contact.

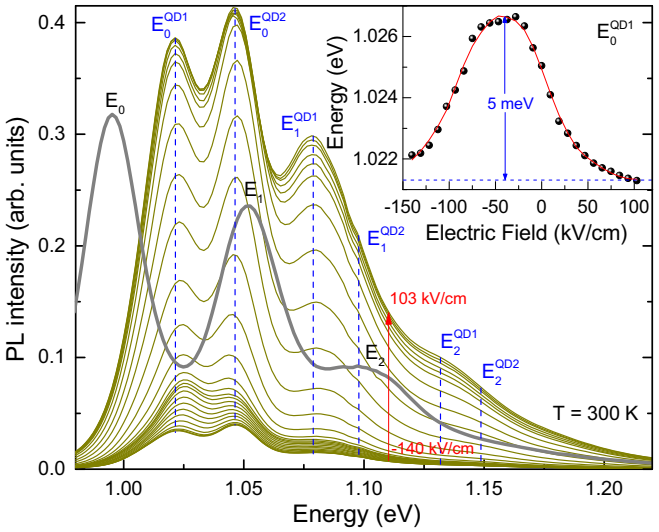

FIG. 2. Room temperature photoluminescence spectra of *Sample 2*, measured with an excitation power of 5 mW. The E_0 peaks from the two dot layers are observed to be energetically separated by 24 meV. With the application of the bias on the gate, both peaks show a clear indication of Stark shift. Inset: A Stark shift of 5 meV is found when the bias on the gate is tuned from −3 V to 2 V. The thick gray curve is the PL spectrum of *Sample 1* under zero bias condition.

The voltage-dependent PL measurements of *Sample 2* at room temperature are presented in Fig. 2. For comparison, the PL spectrum of *Sample 1* with a single QD layer at zero gate bias is plotted as a thick gray line. A clear blueshift of approximately 26 meV is seen in the complete spectrum of bilayered-QD sample (*Sample 2*) compared to the single QD-layered sample (*Sample 1*), reported before [39], and is ascribed to the strain between the layers in a QDM sample in comparison to the monolayered sample. Moreover, the recombination energy in the second layer is blueshifted compared to the first layer that results from the vertical stacking of dots, leading to thinner and wider QDs in the second layer compared to the first layer [39,40]. It can also be observed that while there are only three distinct peaks present in the monolayered sample, the bilayered sample has six peaks. The additional peaks correspond to the recombination of electron-hole pairs in the second QD layer [21]. While a clear splitting of the E_0 transition is seen in *Sample 2*, the E_1 transition only broadens and a small shoulder is registered at around 1.1 eV. On increasing the voltage from −3 V to 2 V, no clear splittings of the QD states are observed that would indicate the coupling between the two layers of QDs, other than a Stark shift. For example, a Stark shift of 5 meV is observed for the first peak corresponding to QDs in the first layer (E_0^{QD1}) and is shown in the inset of Fig. 2. It is noteworthy to mention that there is a comparable shift for the second *s* peak but in the opposite direction. This is an indication of the indirect transition between electrons in the second layer and holes in the first layer that we assist to the Coulomb coupling between the two QD layers. Due to the thermal broadening of the transitions at room temperature, it becomes rather difficult to observe a clear effect of the anticrossing as the gate bias is tuned. Apart from the clear broadening of the E_1 peaks, they show a strong blueshift with negative biases. However, the PL ensemble inhomogeneity of approx. 20 meV indicates that despite findings of other groups, we are dealing with a rather homogeneous ensemble. Using a simple lever-arm calculation, it is found and experimentally observed that the anticrossings occur at negative electric fields with a magnitude according well to the distance between the dots for electron tunneling [26]. Further signatures of electron tunneling/coupling supporting the above statement have also been observed in the electrical characterization described later [33,34].

The contour plots of voltage-dependent PL spectra at 77 K for the two QDM samples: *Sample 2* where the QD layers are separated by 11 nm and *Sample 3* where the separation is 9 nm are presented in Figs. 3(a) and 3(b) while the corresponding spectra at different gate voltages showing the splitting manifested within the broad spectral linewidths of the ensemble are plotted in Figs. 3(c) and 3(d), respectively. For *Sample 2*, the observed splitting is only 3 meV which is predominantly masked by the Stark splitting at room temperature. On the contrary, in the case of *Sample 3* the splitting is 5 meV. The splitting is a manifestation of coupling between the ground state direct and indirect transitions of the two QD layers that decreases exponentially with an increase of the distance between the two dot layers (see Supplemental Material [41]). With the application of the bias, the direct and indirect transition energies between the two QD layers can be brought in resonance where new states are formed. These states can be visualized as the bonding and the antibonding states [1–3] with energies slightly higher and lower than the E_0 recombination energy, thus leading to a splitting. For a sample with an ensemble of QDs in each layer, this can be seen very clearly by using voltage-dependent micro-PL measurements [1]. In the present study, the goal is however not to characterize the formation of such coupled states optically but electrically via the C-(V) spectroscopy and to report the formation of neutral and charged indirect exciton complexes in such coupled QDMs. Before we go into the details, it is necessary to understand the C-(V) spectra of a coupled QDM and to correctly assign the observed signatures to the quantized states in the molecule.

IV. SUPPRESSION OF QD STATES

In C-(V) spectroscopy, the capacitance between the top and the back contacts is measured as a function of the DC bias applied to the gate. As the bias is increased, the quantized electronic states can be shifted down with respect to the quasi-Fermi level (more precisely, the chemical potential) associated with the back contact. When the states are in resonance with the reservoir, electrons tunnel between the dots and the reservoir in accordance with the modulation frequency. Thus subsequent charging of the QD states with electrons is registered as an increase in the capacitance between the top and the back contact, featuring a peak in the C-(V) spectrum. The C-(V) spectrum of a single QD layer (*Sample 1*) is shown in Fig. 4(a) and the corresponding nomenclature for the charging peaks is depicted in Fig. 4(b). The separation between the two *s* peaks gives us the value of the Coulomb blockade (or the Coulomb repulsion energy, E_C^{ss}) between the two *s* electrons.

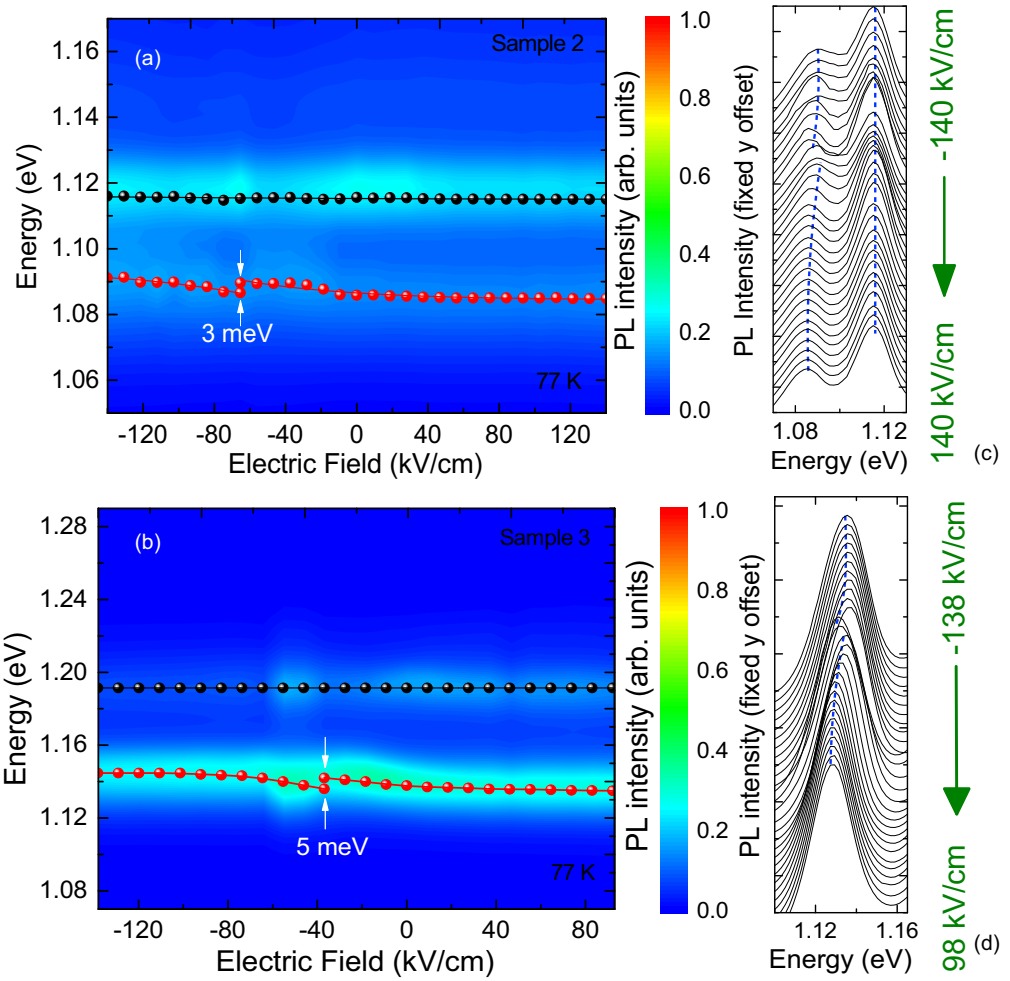

FIG. 3. Contour plot of the photoluminescence spectra measured at 77 K as a function of the gate biases for QDM samples where the QD layers are separated by (a) $d = 11$ nm (*Sample 2*) and (b) $d = 9$ nm (*Sample 3*). The inhomogeneously broadened linewidths originate from an ensemble of QDs. The QD states split as a function of the gate voltage. The strength of the splitting is 3 meV when the QD layers are separated by 11 nm. On reducing the distance between the two layers to 9 nm, the splitting is 5 meV, which results from a better overlap of the QD states in the two layers and hence better coupling. The spectra for different bias values for (c) *Sample 2* and (d) *Sample 3*, are plotted with a fixed offset to show the splitting of the peaks manifested within the broadened linewidths of the transition. The blue-dashed lines are a guide to the eye.

The energetic spacing ($E_{s\to p}$) between the quantized s and p levels can be obtained from the separation of s_2 and p_1 peaks using the relation [22,31]:

$$E_{s_2} - E_{p_1} = E_{s\to p} + \tfrac{1}{4}E_C^{ss}, \tag{2}$$

where E_{s_2} and E_{p_1} are the bias-dependent electrostatic energies corresponding to s_2 and p_1 peaks, respectively, obtained by using Eq. (1). The sequence of charging—$s_1(\uparrow)$; $s_2(\downarrow)$; $p_1(\uparrow)$; $p_2(\downarrow)$; $p_3(\uparrow)$; $p_4(\downarrow)$—is in accordance with Hund's rule and has been extensively demonstrated by time-resolved transconductance spectroscopy [42].

The frequency-dependent C-(V) spectra of *Sample 2* and *Sample 3* are plotted in Figs. 4(c) and 4(d), respectively. It can be seen that as the frequency of the AC signal is increased to several hundreds of kHz, the charging signature of the s electrons on the C-(V) spectrum disappears. This can be explained as follows: With higher modulation frequency, the modulation time reduces and when it becomes lower than the charging/tunneling time, the electrons fail to tunnel in and out resulting in a reduction of the measured capacitance. Since the tunneling time for p electrons is six times faster than that of s electrons [43], this results in the failure of s electrons to respond with higher modulation frequencies and consequently a decrease in the capacitive signal. Thus, the frequency-dependent C-(V) spectroscopy is performed to identify the charging peaks that correspond to the s electrons. These measurements uniquely separate out the s peaks from the p peaks. In both samples, the s states of the second QD layer are suppressed significantly that results from the larger distance of the second layer from the reservoir of electrons; the tunneling probability reduces with the increase of the modulation signal frequency. In both the samples similar suppression of the s peaks of the first QD layer is observed. For *Sample 2*, where the second QD layer is much farther from the reservoir, the s peaks are completely suppressed at much lower frequencies in comparison to *Sample 3* where the second QD layer is nearer. All measurements in this section are performed using an LCR meter, while for the following

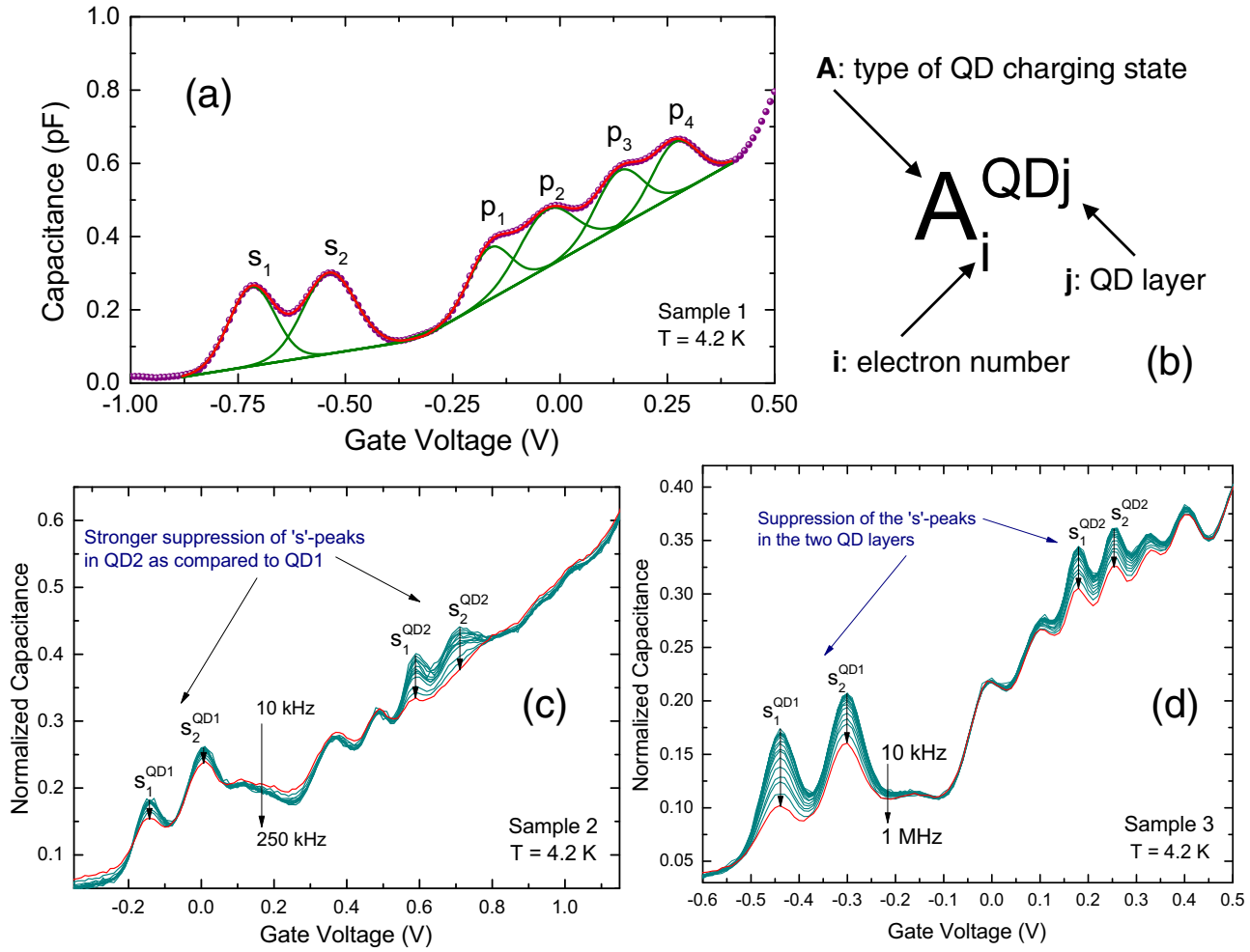

FIG. 4. (a) C-(V) spectra of the sample with a single layer of QD (*Sample 1*). (b) The adopted nomenclature for peak assignments. Capacitance measured as a function of the gate voltage at 4.2 K under different modulation frequencies of the AC signal for (c) $d = 11$ nm (*Sample 2*) and (d) $d = 9$ nm (*Sample 3*). The values of the measured capacitance are normalized to [0,1], such that they overlap on one another in order to observe the suppression of the charging peaks with an increase of the modulation frequency. While a strong suppression is observed for the *s* peaks of the second QD layer in both the samples, the suppression of the *s* peaks in the first layer for the *Sample*2 is much less than in *Sample*3. Besides, much higher modulation frequencies (nearly 1 MHz) are required for the suppression of the *s* peaks of the second dot layer, when the two dot layers are closer as compared to the sample where the dot layers are farther (250 kHz).

sections lock-in measurement scheme is used. In all spectra of Figs. 4(c) and 4(d), normalized capacitances are plotted, where normalization is carried out across the complete measured voltage range (i.e., −2 V to 1 V). This is performed in order to visualize the suppression of the *s* peaks on a common scale. The charging sequence of the peaks is very similar owing to similar structure design. The approximate density of SAQDs in both layers can be calculated from the area under the C-(V) curve after subtracting the background capacitance [22]. The density of SAQDs in *Sample 1* is 1.24×10^9 cm^{-2}. The density of QDs in the second layer for both QDM samples is slightly lower than the first layer. For *Sample 2*, the density of SAQDs is 2.48×10^9 cm^{-2} in the first layer and 1.7×10^9 cm^{-2} in the second layer, while for *Sample 3*, it is 1.79×10^9 cm^{-2} in the first layer and 1.12×10^9 cm^{-2} in the second layer.

The position of each charging peak remains fixed and is not influenced by the change of the modulation frequency. In *Sample 3*, the C-(V) spectra are shifted more to negative voltages. This arises purely from the structure design that results from a different separation of the QD layers in the two samples. The Coulomb repulsion energies and the energetic separation between the quantized levels in all three samples are listed in Table I. These values are calculated for a modulation frequency of 2.33 kHz using lock-in detection scheme. A Coulomb interaction energy of around 20 meV is found in *Sample 1* and in both QD layers of *Sample 2*. This energy value has been reported before for a single layer of InAs SAQDs [22,31,35]. A significant reduction in the value of Coulomb energy is observed in the second QD layer of *Sample 3*. This can be explained as a contribution of two dominant exchange interactions: first between the *s* electrons of the two dot layers and second between the first *s* electron of the second QD layer with the two *p* electrons of the first layer that reduces the Coulomb interaction between the *s* electrons of the second layer. In order to quantify this, it is necessary to calculate the

TABLE I. Coulomb energies and the intersubband, $s \rightarrow p$, resonance energies calculated for both QDM samples using the simple lever arm rule. All values are in meV.

	$\Delta E^{QD1}_{s_1\|s_2}$	$\Delta E^{QD1}_{s_2\|p_1}$	$\Delta E^{QD2}_{s_1\|s_2}$	$\Delta E^{QD2}_{s_2\|p_1}$
Sample 1				
E_C^{ss}	19.6 ± 0.1			
$E_{s\rightarrow p}$		40.1 ± 0.6		
Sample 2				
E_C^{ss}	19.6 ± 0.1		21.0 ± 0.1	
$E_{s\rightarrow p}$		45.6 ± 0.6		40.8 ± 0.3
Sample 3				
E_C^{ss}	21.3 ± 0.1		13.5 ± 0.5	
$E_{s\rightarrow p}$		38.3 ± 0.7		46.0 ± 0.3

dot-dot interaction that is Coulombic in nature. This can be evaluated using the following approximation [33,34]:

$$E_{C\text{-}dot\text{-}dot} = \frac{e^2}{4\pi\epsilon_0\epsilon}\left(\frac{4}{d} - \frac{4}{2t_1 + d} - \frac{1}{2(t_1 + d)}\right), \quad (3)$$

where $E_{C\text{-}dot\text{-}dot}$ is the Coulomb energy between four electrons in the first dot layer and the first electron in the second layer. This is purely based on the electrostatic approach, and the last term in the above equation is introduced to account for the effect of the mirror charge in the back contact [33]. On the charging order of our QDMs: The charging of the s peaks from the second QD layer occurs before the charging of the third and fourth p peaks of the first layer—a characteristic feature of the coupling between the two dot layers [33]. Using the above relation (for example in the case of *Sample 3*) with $d = 9$ nm, $t_1 = 33$ nm, and $\epsilon = 12.9$, the dot-dot Coulomb energy is 42 meV. With the lever-arm rule, this corresponds to a voltage shift of 0.3 V. This implies that the Coulomb interaction between the two dot layers in the sample would shift the position of the charging peaks of the second layer by 0.3 V. Without this interaction the first s peak would be observed at -0.15 V. The presence of a small shoulder in the C-(V) spectra at -0.15 V could feature the charging of uncoupled dots in the subensembles for *Sample 3* and at 0.15 V for *Sample 2*.

For smaller QDs of the subensembles, with a smaller confinement in the first QD layer, the tunneling barrier is smaller and so the peak gets suppressed at higher frequencies. For *Sample 2*, the separation between the dot layers does not introduce any change in the Coulomb interaction between the s electrons of the second layer. However, for *Sample 3*, there is a significant change: The Coulomb interaction in the second layer is reduced by 8 meV. This can be qualitatively explained as contributions from exchange interactions as mentioned above. It is to be noted that there are two p electrons in the first layer and one s electron in the second layer. The exchange interaction, $E^X_{p_{QD1}s_{QD2}}$, can be expressed as [44]:

$$E^X_{p_{QD1}s_{QD2}} = \frac{e^2}{4\pi\epsilon_0\epsilon}\iint \frac{\psi^e_{p_{QD1}}(\vec{r}_1)^*\psi^e_{s_{QD2}}(\vec{r}_2)^*\psi^e_{p_{QD1}}(\vec{r}_2)\psi^e_{s_{QD2}}(\vec{r}_1)}{|\vec{r}_1 - \vec{r}_2|} \times d\vec{r}_1 d\vec{r}_2, \quad (4)$$

where $\psi^e_{p_{QD1}}(\vec{r})$ and $\psi^e_{s_{QD2}}(\vec{r})$ are the basis states for electrons in the first and the second QD layers, respectively. Qualitatively, the dot-dot dependency is taken care by $|\vec{r}_1 - \vec{r}_2|$. The exchange interaction between the s electrons of the two dot layers can be written in a similar format. Here, we arrive at one of the unique features of the C-(V) spectra of a QDM sample where the Coulomb-dominated interaction between the two layers can be identified. In addition, the separation between the s and p level of the first layer in *Sample 3* is significantly reduced. Typically, for our QD samples under standard growth conditions as mentioned before, the infrared transmission measurements show that the quantized states are separated by approximately 45 meV [22]. For further assignment of the charging peaks, magnetic field dependent C-(V) spectroscopy is performed, where the p peaks shift with higher magnetic fields as a result of the orbital Zeeman effect. This phenomenon along with the rearranging of filled states upon application of perpendicular magnetic field together with Landau fan of two-dimensional electron gas in the wetting layer are presented in the next section.

V. MAGNETO-C(V)

The quantized energy levels in quantum dots can be considered as shells in an atom where the s level has twofold spin degeneracy while the p level has twofold orbital and twofold spin degeneracy. In the presence of a perpendicular magnetic field the twofold orbital degeneracy of the p level can be lifted due to orbital Zeeman effect [33–35,45]. This analysis strongly supports the previous assignment of the charging p peaks in the C-(V) spectrum of the QDM samples. The lifting of the orbital degeneracy scales with the applied magnetic field and with the cyclotron frequency. According to Fock's theory, the energy $E_{0,l}$ is given by [45,46]:

$$E_{0,l} = (|l| + 1)\hbar\sqrt{\omega^2_{s\rightarrow p}\big|_{B=0} + \left(\frac{\omega_c}{2}\right)^2} \pm l\hbar\frac{\omega_c}{2}, \quad (5)$$

where $l = \pm 1$ corresponding to the two orbitally degenerate p levels. Thus, the energy difference can be explained using the following relation:

$$\frac{\Delta E}{\hbar} = \omega_{\pm} = \sqrt{\omega^2_{s\rightarrow p}\big|_{B=0} + \left(\frac{\omega_c}{2}\right)^2} \pm \frac{\omega_c}{2}, \quad (6)$$

where $\omega_c = \frac{eB}{m^*}$ is the cyclotron frequency and $\hbar\omega_{s\rightarrow p}$ is the spacing between the s and p levels within the conduction band at zero magnetic field. From the slope of the linear dependence, the effective mass m^* can be calculated that is found to be $0.05\ m_0$ with $m_0 = 9.1 \times 10^{-31}$ kg. Upon simplification, the above equation reduces to: $\Delta\omega = \omega_c = \frac{eB}{m^*}$. Figure 5(a) shows the C-(V) spectra of *Sample 3* as a function of the magnetic field. The Zeeman splittings in the first QD layer are plotted as a function of perpendicular magnetic field in Fig. 5(b). The magneto-C-(V) of *Sample 2* is presented in the Supplemental Material [41]. No dispersion is observed in the s levels in either of the QD layers in *Sample 3* since for an s-like ground state the orbital momentum is zero. However, there is a small shift of the s_2^{QD2} towards higher voltage with an increase in the magnetic field [see inset of Fig. 5(a)]. This can be explained as follows: Normally, one would expect the following sequence

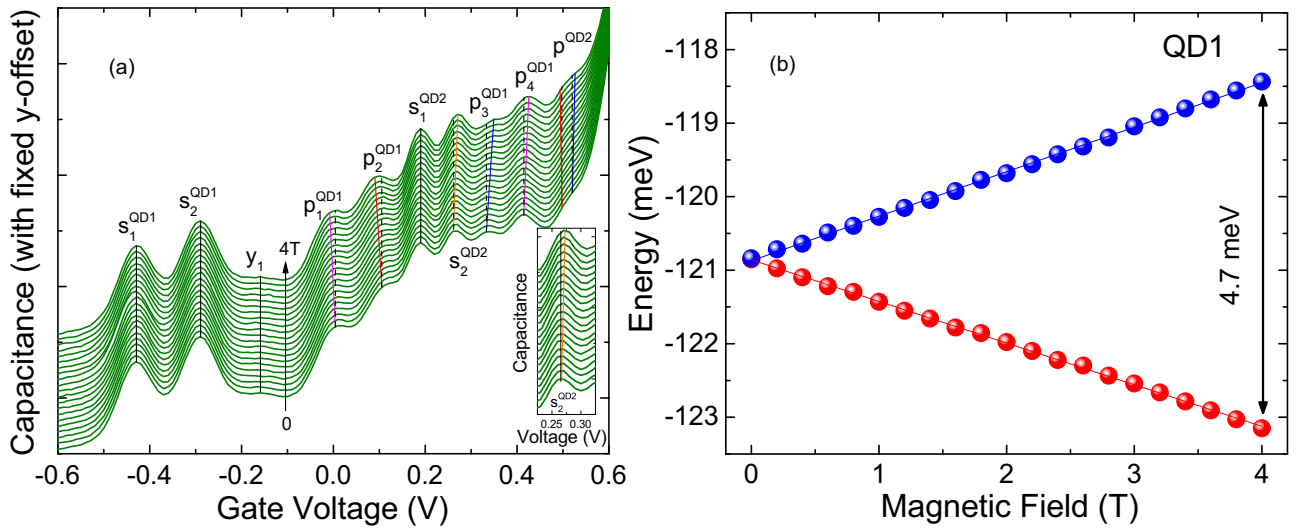

FIG. 5. (a) Capacitance-voltage spectra measured as a function of increasing magnetic field for *Sample 3* ($d = 9$ nm) at 4.2 K, plotted with a fixed y offset. The two s peaks of the first QD layer and the first s peak of the second QD layer did not shift with increasing magnetic field, while the second s peak shows a slight shift as the magnetic field is increased (see inset). (b) Zeeman shift of the p peaks (i.e., p_x and p_y) is observed for the first QD layer. At 4 T, the Zeeman splitting is 4.7 meV. The modulation frequency of the AC signal for all the spectra is kept constant at 1.33 kHz.

for filling of the electrons in the QD layers:

$$s_1^{QD1}(\uparrow); s_2^{QD1}(\downarrow); p_1^{QD1}(\uparrow); p_2^{QD1}(\downarrow); s_1^{QD2}(\uparrow); s_2^{QD2}(\downarrow).$$

However, obeying the Hund's rule, we speculate the following sequence:

$$s_1^{QD1}(\uparrow); s_2^{QD1}(\downarrow); p_1^{QD1}(\uparrow); \underline{p_2^{QD1}(\uparrow)}; s_1^{QD2}(\uparrow); s_2^{QD2}(\downarrow).$$

This leads to a lower separation between the s state of the second QD layer and p state of the first layer at zero magnetic fields. Upon increasing the magnetic field, $p_2^{QD1}(\downarrow)$ is energetically more favored. This would lead to an increase in the spacing and thus would eventually lead to the shifting of s_2^{QD2} to higher voltages (or higher energies). Similar behavior has also been reported before by Luyken *et al.* [33].

The p states in both the layers show distinct well-known magnetic dispersion, characteristic to the orbital Zeeman effect. In *Sample 3*, the dispersion in the p levels is observed clearly in the first QD layer. The charging of the wetting layer in the second QD layer smears out the charging p peaks and hence it is difficult to quantify the Zeeman splitting in the second layer. A splitting of 4.7 meV is observed at 4 T [see Fig. 5(b)] that also scales with the magnetic field. For *Sample 2*, at 5 T, the observed splitting in the first layer is 3.4 meV while that of the second layer is 5 meV (see Supplemental Material [41]). The charging of the s states in the second QD layer occurs before the complete charging of the four electrons in the p states of the first layer. At first, it might seem that at zero magnetic fields, there is no orbital degeneracy of the p states. However, it has been shown that even at zero magnetic fields the orbital degeneracy in the p states takes a nonzero value [37,47]. Correcting for this nonzero value as 15 μeV, the linear dispersion for p states is plotted in Fig. 5(b) for *Sample 3*. The charging peaks marked as y_1 in the first layer of *Sample 3* at $V_g = -0.15$ V show no dispersion with the increasing magnetic field [see Fig. 5(a)]. As explained before, these peaks are associated with the charging of uncoupled dots in the ensemble for *Sample 3*. The nondispersive nature of these peaks shows its s-like nature for the ensembles in the sample.

At voltages higher than 0.7 V for *Sample 3*, the formation of 2D-Landau levels in the wetting layer is observed that scales with the magnetic field as shown in Figs. 6(a) and 6(b). At zero magnetic field, the discrete and strongly degenerate density of states transit to a continuum. With a decrease of the magnetic field, the Landau levels decrease their separation and eventually form this constant 2D density of states [48], forming a Landau fan. This is used to calculate the Fermi energy level as $E_F = \frac{\pi\hbar^2}{m^*}N_{2D}$. The 2D carrier density can be calculated from the gate voltage where the black-dashed lines in Fig. 6(b) meet at zero magnetic field, using the relation:

$$N_{2D} = \frac{\epsilon V_g}{el} = 72.4 \times 10^{12}\,\mathrm{cm}^{-2}\frac{V_g(V)}{l(nm)}. \quad (7)$$

With $l = 156$ nm (the distance of the wetting layer from the top gate), and $V_g = 0.56$ V, we get $E_F = 9$ meV. Three Landau levels from the wetting layer are identified and are marked as LL_1^{WL}, LL_2^{WL}, and LL_3^{WL} as in Fig. 7(b).

VI. OBSERVATION OF INDIRECT EXCITONS

When the capacitance of a QD sample is measured as a function of gate voltage under illumination with an NIR-LED (center wavelength at 950 nm), signatures of excitonic peaks are observed before the charging of the s states [35]. The LED is placed in close proximity to the sample. The spot size is approximately 4 mm. The light intensity is calibrated with a power meter and is found to be proportional to the LED current (i.e., 24 W/m^2 per 1 mA of current applied to the LED) for the range used in the measurements. The strength of the peaks depends on the illumination power that is characterized by the amount of constant current applied to the LED. Under

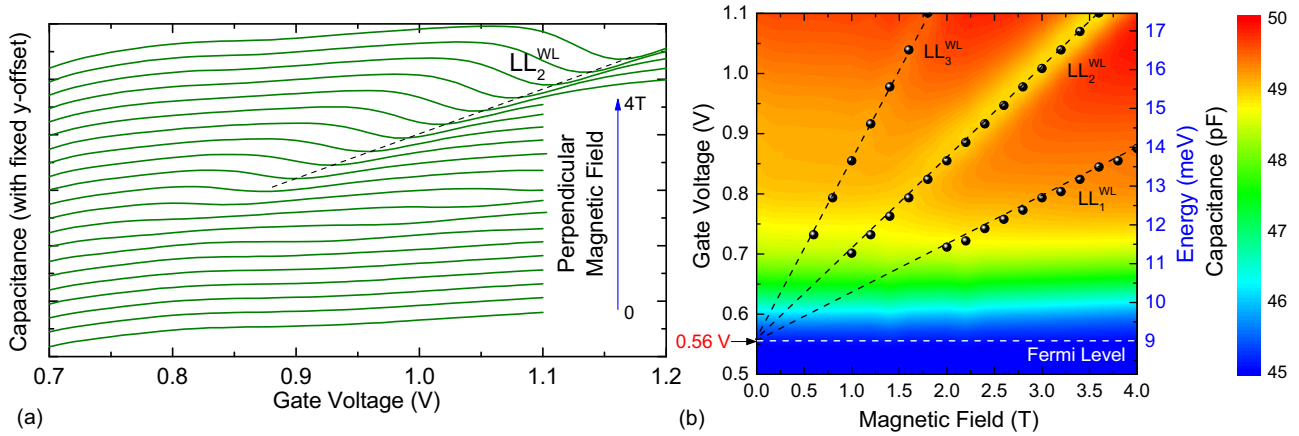

FIG. 6. (a) Capacitance-voltage spectra measured as a function of increasing magnetic field for *Sample 3* ($d = 9$ nm) at higher gate biases ($V_g \geqslant 0.7$ V). Two-dimensional electron gas (2DEG) channels are formed in the wetting layer, resulting in the observation of Landau levels that shifts with an increase of the magnetic field. These are marked with black-dashed lines. (b) The corresponding contour plot showing the fan-out diagram of three Landau levels marked as LL_1^{WL}, LL_2^{WL}, and LL_3^{WL}.

illumination, the situation becomes much more complicated where the resonance condition [32] of charging peaks will be determined by the energy of the electrons in the ground state and the electron-hole interaction energies [35]. This, however, is valid for a single layer of QD in the MIS-Schottky diode device design. In the case of two QD layers, as for the QDMs, the resonance condition will be given by the electrons in the ground state of the first QD layer and the electron-hole interaction energies between the two dot layers (i.e., electron in the first layer and holes in the second layer). This implies that the strength of the coupling between the two dot layers and hence the distance between the layers will play an important role. When the sample is illuminated, the complex current that is measured not only contains the capacitive signal purely from the QD charging but also the photocurrent generated by the LED. Thus at this stage, it is difficult to infer any valid conclusions from the measured height of the capacitance under different illumination power. Before moving into the results from the QDM samples, we first discuss the results from the single QD layer (*Sample 1*).

Figure 7(a) shows the C-(V) spectra of *Sample 1* with different illumination intensities characterized by the LED current. Clearly, without any illumination, there are no exciton charging peaks and they start to appear as the constant current through the LED is increased. In addition to the charging of the *s* states, we could resolve five additional peaks in the reverse bias direction. The peaks induced by illumination can be related to the charging of QDs occupied by the photogenerated holes. A larger reverse bias and a higher LED current is necessary for the generation of more holes to observe the

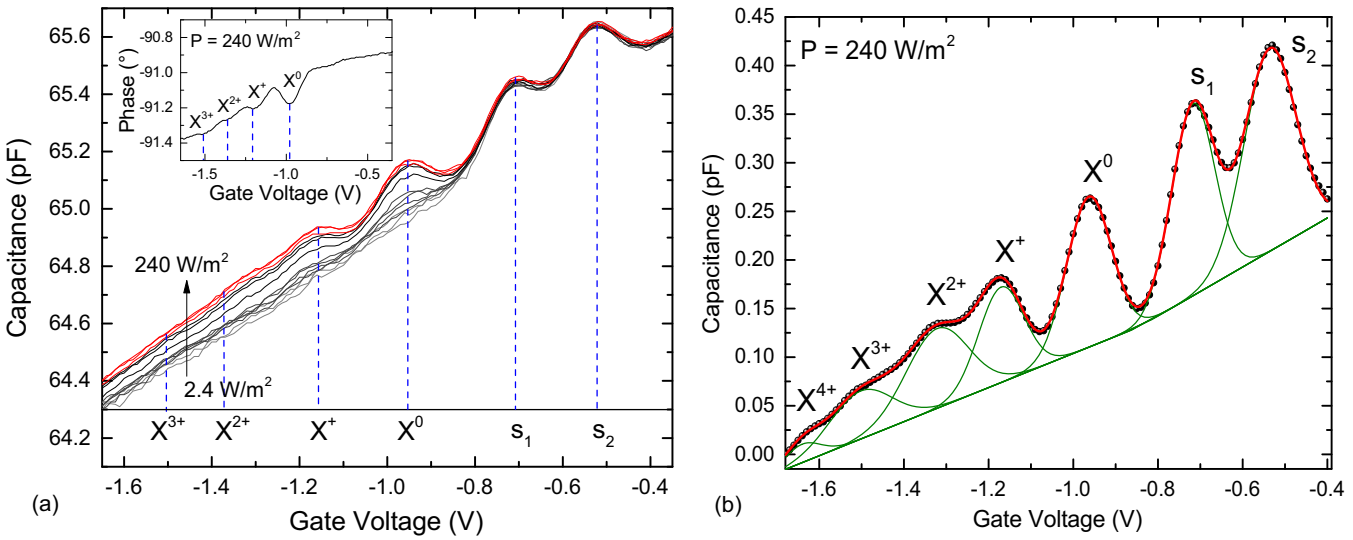

FIG. 7. (a) Capacitance-voltage spectra measured as a function of increasing LED current (I_{LED}) for *Sample 1* (single QD layer) at 4.2 K. The modulation frequency of the AC signal for all the spectra is kept constant at 433 Hz. With an increase in the LED current, new exciton charging peaks are observed for gate biases, $V_g \leqslant -0.8$ V. Inset: The phase measured for the corresponding voltage range of the C-(V) spectrum that shows dips at the gate biases where exciton peaks appear. (b) The deconvolution of the C-(V) curve for $I_{LED} = 10$ mA (corresponding to a power density of 240 W/m^2) showing neutral and charged direct exciton peaks.

TABLE II. Direct interaction energies calculated for the single QD layer (*Sample 1*) using the simple lever arm rule. All values are in meV. These values are calculated for an illumination intensity of 240 W/m^2 [see the deconvoluted peaks in Fig. 7(b)]. E_{ES} represents the electrostatic energy corresponding to each gate voltage and $J_{e_0h_i}$ is the direct Coulomb interaction energy between the electron tunneling into the orbital s state e_0 and the additional hole residing in the single particle state h_0 (for X^0, X^+), h_1 (for X^{2+}, X^{3+}), or h_2 (for X^{4+}).

Peak complexes	Interaction type	Value
$\Delta E_{s_2\|s_1} = E_{ES}^{s_1} - E_{ES}^{s_2}$	E_{ss}^{C}	20.8 ± 0.1
$\Delta E_{s_1\|X^0} = E_{ES}^{X^0} - E_{ES}^{s_1}$	$-J_{e_0h_0}$	27.8 ± 0.2
$\Delta E_{X^0\|X^+} = E_{ES}^{X^+} - E_{ES}^{X^0}$	$-J_{e_0h_0}$	24.3 ± 0.2
$\Delta E_{X^+\|X^{2+}} = E_{ES}^{X^{2+}} - E_{ES}^{X^+}$	$-J_{e_0h_1}$	17.4 ± 0.4
$\Delta E_{X^{2+}\|X^{3+}} = E_{ES}^{X^{3+}} - E_{ES}^{X^{2+}}$	$-J_{e_0h_1}$	20.8 ± 0.5
$\Delta E_{X^{3+}\|X^{4+}} = E_{ES}^{X^{4+}} - E_{ES}^{X^{3+}}$	$-J_{e_0h_2}$	16.2 ± 0.5

higher charged excitons. The inset of Fig. 7(a) shows the phase as a function of the gate voltage. Whenever an exciton charging is registered in the capacitance, consecutively, there is a drop in the phase. Figure 7(b) presents the deconvolution of all the peaks observed when a current of 10 mA (240 W/m^2) is applied to the LED. It can be seen that the peak height decreases with higher reverse bias. This can be explained as follows: As more reverse bias is applied, the QD is charged with more holes resulting in an increase of the net positive charge of the QD. This increasing positive charge will thus create a repulsive barrier that will reduce the rate of capture of holes outside the QDs. Stronger electric field and thus a lowered barrier would, in turn, lead to faster out-tunneling of the electrons from the wetting layer and a rather slow in-tunneling of the nonresonant electrons due to image charges. Consecutively this results in the decrease of the height of successive higher charged exciton peaks. To extract the charging energies corresponding to each of the peaks, the respective voltages are converted to energies (see Table II) using the simple lever arm rule mentioned before.

While these phenomena have been recently demonstrated elaborately [35], the situation with two layers is very different, which we are not able to explain at this point by simple models. Hence we explain our findings on the quantum-dot molecule

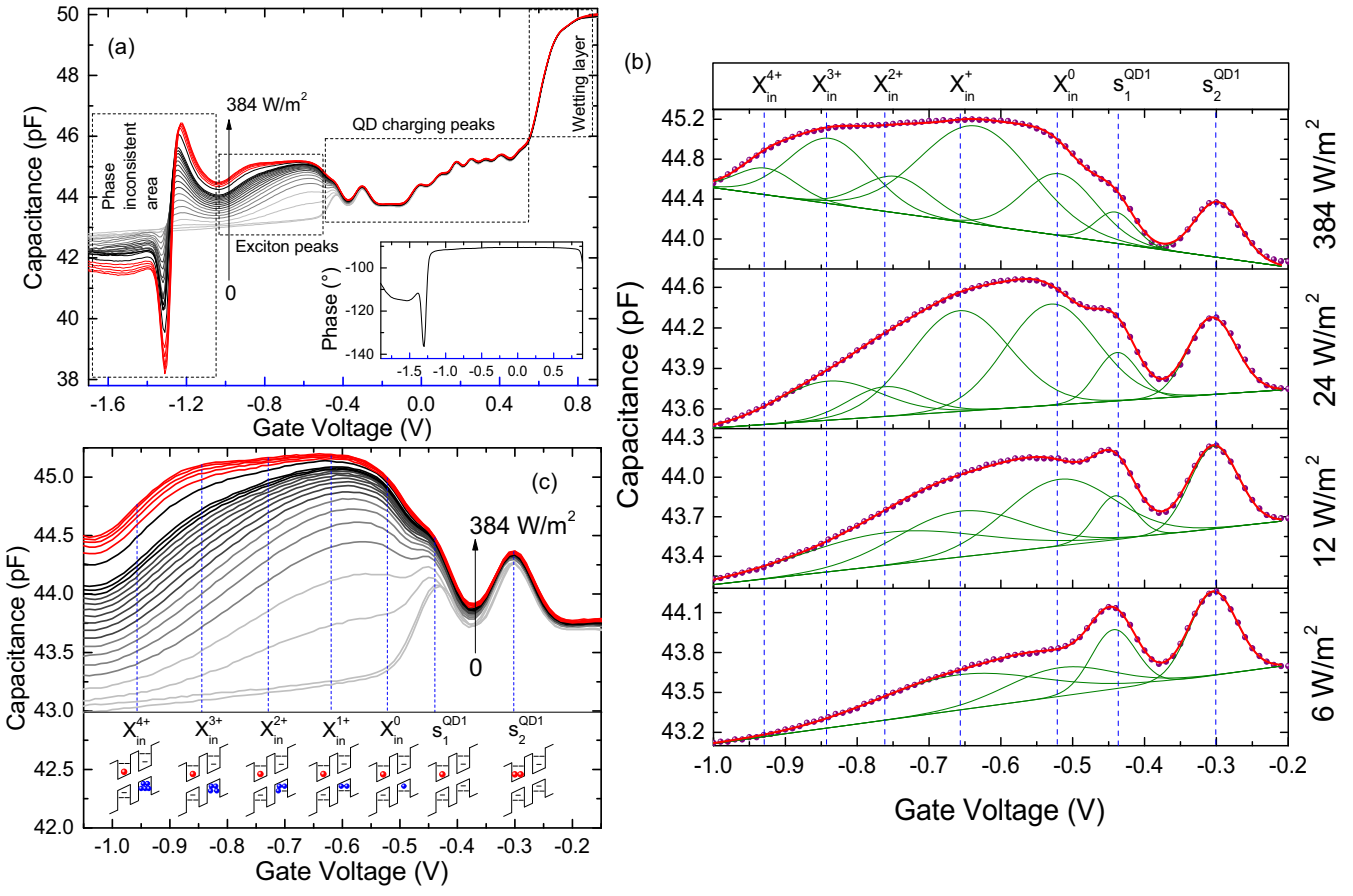

FIG. 8. (a) Capacitance-voltage spectra measured as a function of increasing LED current (I_{LED}) for *Sample 3* ($d = 9$ nm) at 4.2 K. The modulation frequency of the AC signal for all the spectra is kept constant at 433 Hz. The whole charging spectra are divided into four parts that comprises the phase unstable region, exciton charging peaks, QD charging peaks, and the charging of the wetting layer, indicated by dashed boxes. Inset: The phase measured for the complete voltage range of the C-(V) spectra. (b) The deconvolution of the C-(V) curves for four different I_{LED} showing the neutral and the charged indirect exciton peaks arising from the crossed-recombination of electrons and holes between the two QD layers. (c) The evolution of the neutral and charged indirect exciton peaks as a function of the LED current, with a possible crossed-recombination scheme shown schematically under each charging peak observed for -1 V $\leqslant V_g \leqslant -0.2$ V. The schematic representation depicts only one of the possible charge configurations, while the rest are mentioned in the Supplemental Material [41].

samples in the following, qualitatively. Distinct features of the C-(V) spectra under different illumination intensities for *Sample 3*, where the two dot layers are 9 nm apart, are shown in Fig. 8(a). Briefly, three charging regions can be separated: the QD charging peaks, the wetting layer charging, and the charging of the indirect excitons. For gate biases, $V_g \leqslant -1$ V, the region is phase inconsistent and hence this is not considered for investigation. The measured phase of the complex current is plotted in the inset of Fig. 8(a) that justifies the above statement. The observation of this feature below -1 V is assisted to the charging of the WL of the second QD layer with holes. In Fig. 8(b), the spectral deconvolutions are shown for four different LED currents: 0.25 mA (6 W/m^2), 0.5 mA (12 W/m^2), 1 mA (24 W/m^2), and 16 mA (384 W/m^2), to show the evolution of the indirect excitonic peaks with the increasing illumination intensity. Figure 8(c) shows the C-(V) spectra for a series of increasing LED current from 0 to 16 mA. The schematic below each peak corresponds to the characteristic representation of the indirect exciton formation with the electron in the s state of the first QD layer and a varying number of holes in the valence band of the second QD layer. Quite similar but yet different features are observed for *Sample 2* [see Figs. 9(a) and 9(b)] where the QD layers are separated by 11 nm. The shoulder peak marked as y_1 has already been explained before while the origin of the other peak marked as y_2 is not well understood. In both cases, as the illumination intensity is increased, the s_1 peak of the first QD layer is lifted up and smears into the exciton charging peaks. While this occurs in the case of *Sample 2* at lower illumination intensities, for *Sample 3* much higher illumination intensities are required. The situation is contrary to what is observed in *Sample 1* where the magnitude of the s peaks does not change. This is a consequence of *illumination-induced nonequilibrium hole-discharging effect* and is explained as follows: Under illumination, holes may fill the QDs and eliminate electrons from the QDs at the charging voltage for example at the voltage corresponding to the first s peak. At this voltage, electrons can tunnel in and out of the QDs. However, if the electron is eliminated by an illumination-induced hole, the QD is not in an equilibrium condition when another electron can tunnel in. This phenomenon can happen resonantly leading to the observation of an increase in the capacitance signal, which is further enhanced as the illumination power is increased. The increase in the capacitive signal of the s peak is further assisted by the existence of long-lived nonequilibrium states such as an indirect X^{1-} state. Besides with stronger illumination a slight shift of the peaks to lower voltages results from the weak tunnel coupling in our inhomogeneous QD ensemble owing to deeper confinement energies for larger QDs. All measurements under illumination are performed with a low AC modulation frequency since this prevents the suppression of the excitonic transitions [35] with a flexibility to apply a much higher LED current. Unlike the single QD layer sample, the exciton peaks are quite difficult to distinguish due to multiple possible charge configurations and the nonequilibrium situations due to long-lived indirect excitons.

A careful deconvolution via multiple Gaussian fittings in both cases shows that there are five additional peaks in the reverse bias direction. At first, a low illumination power is applied to the sample to induce less perturbation. Under this situation, only the neutral indirect exciton complex peak appears. This position is noted and kept constant for the subsequent higher illumination intensities. The above procedure is repeated for further increase in the illumination power. In all cases, the linewidths of the peaks are treated as fitting parameters. We note that linewidths of the peaks change with increasing illumination intensity and the observed feature from illumination is rather broad contrary to the

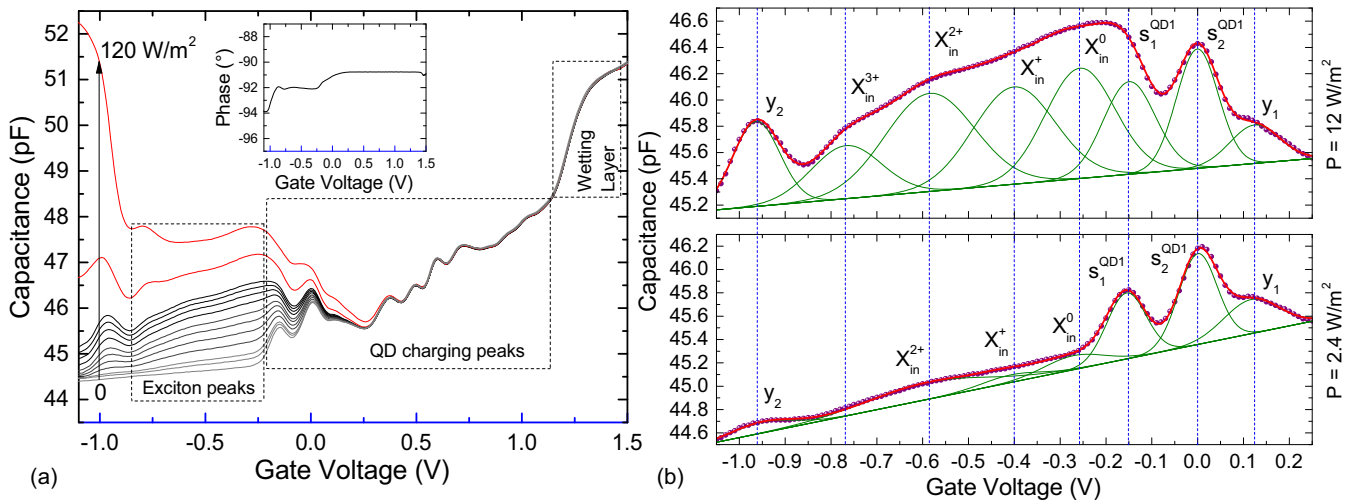

FIG. 9. (a) Capacitance-voltage spectra measured as a function of increasing LED current (I_{LED}) for *Sample 2* ($d = 11$ nm) at 4.2 K. The modulation frequency of the AC signal for all the spectra is kept constant at 533 Hz. With an increase in the LED current while no change is observed in the wetting layer and the QD charging peaks that are comprised of p peaks, new indirect exciton charging peaks are observed for gate biases, $V_g \leqslant -0.25$ V. The whole charging spectra are divided into three parts that are comprised of the exciton charging peaks, QD charging peaks, and the charging of the wetting layer. With high LED currents, $I_{LED} \geqslant 0.5$ mA (12 W/m^2), the C-(V) curve is lifted up leading to the smearing of the s states of the first QD layer. Inset: The phase measured for the complete voltage range of the C-(V) spectra. (b) The deconvolution of the C-(V) curve for $I_{LED} = 0.1$ mA (2.4 W/m^2) and 0.5 mA (12 W/m^2) showing the neutral and the charged indirect exciton peaks arising from the crossed recombination of electrons and holes between the two QD layers.

TABLE III. Indirect interaction energies calculated for the double QD layer (*Sample 2* and *Sample 3*) using the simple lever arm rule of the first QD layer. All values are in meV. These values are calculated for an illumination intensity of 12 W/m^2 [see the deconvoluted peaks in Fig. 9(b)] for *Sample 2* and 384 W/m^2 [see the deconvoluted peaks in Fig. 8(b)] for *Sample 3*. E_{ES} represents the electrostatic energy corresponding to each gate voltage, and $J_{e_0^{(1)}h_i^{(2)}}$ is the indirect Coulomb interaction energy between the electron tunneling into the orbital s state e_0 of the first QD layer and the additional hole residing in the single particle state h_0 (for X_{in}^0, X_{in}^+), h_1 (for X_{in}^{2+}, X_{in}^{3+}), or h_2 (for X_{in}^{4+}) in the second QD layer. The number in the first brackets represents the QD layer. Only one of the possible charge configurations for each complex is considered here, while the rest are mentioned in the Supplemental Material [41].

Peak complexes	Interaction type	Value *Sample 2*	Value *Sample 3*
$\Delta E_{s_2\|s_1} = E_{ES}^{s_1} - E_{ES}^{s_2}$	$E_{ss}^{C(1)}$	19.6 ± 0.1	21.3 ± 0.1
$\Delta E_{s_1\|X_{in}^0}^{QDM} = E_{ES}^{X_{in}^0} - E_{ES}^{s_1}$	$-J_{e_0^{(1)}h_0^{(2)}}$	18.2 ± 0.3	12.1 ± 0.4
$\Delta E_{X_{in}^0\|X_{in}^+}^{QDM} = E_{ES}^{X_{in}^+} - E_{ES}^{X_{in}^0}$	$-J_{e_0^{(1)}h_0^{(2)}}$	19.6 ± 0.4	16.7 ± 0.5
$\Delta E_{X_{in}^+\|X_{in}^{2+}}^{QDM} = E_{ES}^{X_{in}^{2+}} - E_{ES}^{X_{in}^+}$	$-J_{e_0^{(1)}h_1^{(2)}}$	25.2 ± 0.1	18.3 ± 0.1
$\Delta E_{X_{in}^{2+}\|X_{in}^{3+}}^{QDM} = E_{ES}^{X_{in}^{3+}} - E_{ES}^{X_{in}^{2+}}$	$-J_{e_0^{(1)}h_1^{(2)}}$	26.6 ± 0.3	13.7 ± 0.3
$\Delta E_{X_{in}^{3+}\|X_{in}^{4+}}^{QDM} = E_{ES}^{X_{in}^{4+}} - E_{ES}^{X_{in}^{3+}}$	$-J_{e_0^{(1)}h_2^{(2)}}$	–	13.7 ± 0.5

well-separated individual peaks as seen in the single QD layer sample (*Sample 1*). While in a single QD layer sample the pure conduction band states probed by C-(V) spectroscopy show an even reduced linewidth compared to PL (see Pal *et al.* [22]), here the situation is different. The hole energy levels of the QDMs are not perfectly aligned in our ensembles. This adds to the inhomogeneous broadening from the conduction band states. Additionally, the Coulomb attracted excitonic states from different charge configurations (see Supplemental Material [41] for the charge configurations associated with each indirect exciton charging peak) are narrower energetically spaced and thus overlap. The gate voltages corresponding to each of these charging peaks are converted into energies using the simple lever arm rule corresponding to the first QD layer in both the samples. This is considered since the single-particle electronic state is in the first QD layer. These results are summarized in Table III. It is observed that the energetic separation between the s_1 peak of the first QD layer and the neutral indirect exciton in both *Sample 2* and *Sample 3* is much lower as compared to the separation between the s_1 peak of the first QD layer and the neutral direct exciton in the single QD layered sample (*Sample 1*).

On account of coupling between the two layers of QDs, thus forming a molecule, the ground state excitonic binding energy drops drastically (on the order of 4–5 meV). This is a consequence of the transition from direct to indirect Coulomb coupling. A schematic of the different exciton formation is shown in Fig. 10. In the case of a single QD, the exciton formation and the excitonic transition energies are typically affected by the strain-induced changes in the conduction and valence band offsets [49]. In a QDM, there is an inherent symmetry breaking leading to a difference

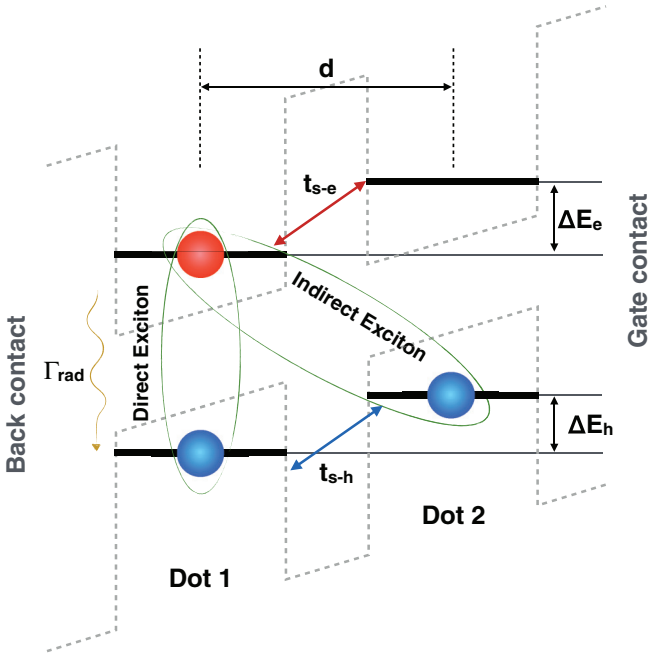

FIG. 10. Schematic of the exciton formation in a quantum dot molecule. The two dot layers are separated by d. $t_{s\text{-}e}$ and $t_{s\text{-}h}$ represent the tunneling strengths of electrons and holes in the conduction and valence band of the QDM, respectively. ΔE_e and ΔE_h are the offset in the conduction and valence bands between the two layers in the QDM and Γ_{rad} represents the direct radiative recombination.

in the confinement potential of holes from one dot layer to the other. As the electric field across the two layers is increased, depending on the direction of the applied field either the hole or electron levels become resonant, leading to the formation of bonding and antibonding states. Since the sample growth has not been targeted to allow tunneling of specific carriers (i.e., either electrons or holes), it is difficult to speculate from the results which carrier-tunneling rate is dominating. Hence, the results are explained only qualitatively to give a flavor of the anticrossings observed in the PL spectra of our samples, while much of the results are focused on the electrical measurements for the observation of indirect excitonic complexes.

VII. CONCLUSIONS

In conclusion, we present a fundamental investigation on quantum dot molecule samples with two different vertical stacking distances. Voltage-dependent photoluminescence at low temperature of the ensemble QDM samples show traces of coupling between the two layers. This results in an anticrossing between the bonding and antibonding states that increases exponentially with a decrease in the distance between the two dot layers, featuring electron tunneling effects. On the other hand, capacitance-voltage spectroscopy proved to be an efficient way to probe QD molecules. On illuminating the samples with an NIR-LED, formation of direct excitons in the monolayer QD sample and indirect excitons in the molecules is observed and quantified. The broad linewidths of indirect excitonic peaks are associated with multiple

possible charge configurations and the presence of long lived nonequilibrium states such as X^{1-}. We have also shown that C-(V) spectroscopy is a powerful tool to probe all electrically the indirect Coulomb coupling dominated charging peaks in the QDMs. With the application of perpendicular magnetic field, a rearrangement of the filling is seen that is manifested as the shift of the orbitally nondegenerate *s* state of the second layer. The charging dynamics of electrons in QDMs is a many-body phenomenon [35,50] that involves a rather complicated electrostatic interaction scheme. With more electrons occupying the energy states of the QDM, the picture is no longer simple, as this will involve complicated exchange interactions between the two layers. As a result of these many-body interactions that involve quantum tunneling and exchange interactions between the layers, throughput theoretical investigations are required to explain our first findings on the indirect exciton charging complexes in QDM samples.

ACKNOWLEDGMENTS

The work is financially supported by the BMBF Quantum communication program - Q.com-H 16KIS0109 and BMBF-QUIMP 16BQ1062 as well as Mercur Pr-2013-0001. The authors would also like to acknowledge the DFH/UFA CDFA-05-06 Nice-Bochum and RUB Research School. S.P., A.L., and A.D.W. acknowledge gratefully the support within the DFG SFB ICRC - TRR 160 Z1 project.

[1] M. Scheibner, M. Yakes, A. S. Bracker, I. V. Ponomarev, M. F. Doty, C. S. Hellberg, L. J. Whitman, T. L. Reinecke, and D. Gammon, Nat. Phys. **4**, 291 (2008).

[2] E. A. Stinaff, M. Scheibner, A. S. Bracker, I. V. Ponomarev, V. L. Korenev, M. E. Ware, M. F. Doty, T. L. Reinecke, and D. Gammon, Science **311**, 636 (2006).

[3] H. J. Krenner, M. Sabathil, E. C. Clark, A. Kress, D. Schuh, M. Bichler, G. Abstreiter, and J. J. Finley, Phys. Rev. Lett. **94**, 057402 (2005).

[4] J. M. Daniels, P. Machnikowski, and T. Kuhn, Phys. Rev. B **88**, 205307 (2013).

[5] Y. Liu, B. Liang, Q. Guo, S. Wang, G. Fu, N. Fu, Z. M. Wang, Y. I. Mazur, and G. J. Salamo, Nanoscale Res. Lett. **10**, 271 (2015).

[6] E. S. Kannan, G.-H. Kim, and D. A. Ritchie, Appl. Phys. Lett. **95**, 143506 (2009).

[7] P. Bhattacharya and Z. Mi, Proc. IEEE. **95**, 1723 (2007).

[8] L. Nevou, V. Liverini, F. Castellano, A. Bismuto, and J. Faist, Appl. Phys. Lett. **97**, 023505 (2010).

[9] G. Cerulo, L. Nevou, V. Liverini, F. Castellano, and J. Faist, J. Appl. Phys. **112**, 043702 (2012).

[10] F. Troiani, U. Hohenester, and E. Molinari, Phys. Rev. B **62**, R2263 (2000).

[11] J. R. Petta, A. C. Johnson, J. M. Taylor, E. A. Laird, A. Yacoby, M. D. Lukin, C. M. Marcus, M. P. Hanson, and A. C. Gossard, Science **309**, 2180 (2005).

[12] E. Biolatti, R. C. Iotti, P. Zanardi, and F. Rossi, Phys. Rev. Lett. **85**, 5647 (2000).

[13] J. M. Villas-Bôas, A. O. Govorov, and S. E. Ulloa, Phys. Rev. B **69**, 125342 (2004).

[14] G. Schedelbeck, W. Wegscheider, M. Bichler, and G. Abstreiter, Science **278**, 1792 (1997).

[15] P. Borri, W. Langbein, U. Woggon, M. Schwab, M. Bayer, S. Fafard, Z. Wasilewski, and P. Hawrylak, Phys. Rev. Lett. **91**, 267401 (2003).

[16] C. Bardot, M. Schwab, M. Bayer, S. Fafard, Z. Wasilewski, and P. Hawrylak, Phys. Rev. B **72**, 035314 (2005).

[17] G. Ortner, M. Bayer, Y. Lyanda-Geller, T. L. Reinecke, A. Kress, J. P. Reithmaier, and A. Forchel, Phys. Rev. Lett. **94**, 157401 (2005).

[18] Y. B. Lyanda-Geller, T. L. Reinecke, and M. Bayer, Phys. Rev. B **69**, 161308 (2004).

[19] K. Müller, G. Reithmaier, E. C. Clark, V. Jovanov, M. Bichler, H. J. Krenner, M. Betz, G. Abstreiter, and J. J. Finley, Phys. Rev. B **84**, 081302(R) (2011).

[20] M. Heldmaier, M. Seible, C. Hermannstädter, M. Witzany, R. Roßbach, M. Jetter, P. Michler, L. Wang, A. Rastelli, and O. G. Schmidt, Phys. Rev. B **85**, 115304 (2012).

[21] A. Boyer de la Giroday, N. Sköld, I. Farrer, D. A. Ritchie, and A. J. Shields, J. Appl. Phys. **110**, 083511 (2011).

[22] S. Pal, S. R. Valentin, N. Kukharchyk, H. Nong, A. B. Parsa, G. Eggeler, A. Ludwig, N. Jukam, and A. D. Wieck, J. Phys.: Condens. Matter **26**, 505801 (2014).

[23] M. Bayer, P. Hawrylak, K. Hinzer, S. Fafard, M. Korkusinski, Z. R. Wasilewski, O. Stern, and A. Forchel, Science **291**, 451 (2001).

[24] J. Wu, X. Hu, J. Lee, E.-S. Kim, and Z. M. Wang, Adv. Opt. Mater. **1**, 201 (2013).

[25] J. Wang, D. Shang, H. Mao, J. Yu, Q. Zhao, P. Yang, and H. Xing, Physica B **408**, 98 (2013).

[26] A. S. Bracker, M. Scheibner, M. F. Dotty, E. A. Stinaff, I. V. Ponomarev, J. C. Kim, L. J. Whitman, T. L. Reinecke, and D. Gammon, Appl. Phys. Lett. **89**, 233110 (2006).

[27] I. Shtrichman, C. Metzner, B. D. Gerardot, W. V. Schoenfeld, and P. M. Petroff, Phys. Rev. B **65**, 081303 (2002).

[28] S. Fafard, Z. R. Wasilewski, C. N. Allen, D. Picard, M. Spanner, J. P. McCaffrey, and P. G. Piva, Phys. Rev. B **59**, 15368 (1999).

[29] S. Fafard, M. Spanner, J. P. McCaffrey, and Z. R. Wasilewski, Appl. Phys. Lett. **76**, 2268 (2000).

[30] Y. Bessho, Y. Harada, T. Kita, E. Taguchi, and H. Yasuda, J. Appl. Phys. **114**, 033517 (2013).

[31] H. Drexler, D. Leonard, W. Hansen, J. P. Kotthaus, and P. M. Petroff, Phys. Rev. Lett. **73**, 2252 (1994).

[32] Z. M. Wang, *Self-Assembled Quantum Dots* (Springer, New York, 2008), pp. 337–357.

[33] R. J. Luyken, A. Lorke, M. Haslinger, B. T. Miller, M. Fricke, J. P. Kotthaus, G. Medeiros-Ribeiro, and P. M. Petroff, Physica E **2**, 704 (1998).

[34] R. J. Luyken, A. Lorke, M. Fricke, J. P. Kotthaus, G. Medeiros-Ribeiro, and P. M. Petroff, Nanotechnology **10**, 14 (1999).

[35] P. A. Labud, A. Ludwig, A. D. Wieck, G. Bester, and D. Reuter, Phys. Rev. Lett. **112**, 046803 (2014).

[36] G. Medeiros-Ribeiro, D. Leonard, and P. M. Petroff, Appl. Phys. Lett. **66**, 1767 (1995).

[37] M. Fricke, A. Lorke, J. P. Kotthaus, G. Medeiros-Ribeiro, and P. M. Petroff, Europhys. Lett. **36**, 197 (1996).
[38] S. Pal, Ph.D. Thesis, Ruhr-Universität Bochum, 2015.
[39] M. C. Bödefeld, R. J. Warburton, K. Karrai, J. P. Kotthaus, G. Medeiros-Ribeiro, and P. M. Petroff, Appl. Phys. Lett. **74**, 1839 (1999).
[40] S. Y. Shah, N. Halder, S. Sengupta, and S. Chakrabarti, Mater. Res. Bull. **47**, 130 (2012).
[41] See Supplemental Material at http://link.aps.org/supplemental/10.1103/PhysRevB.94.245311 for the exponential dependence of splitting with the distance between the QD layers, analysis of the magneto-C(V) for *Sample 2* and multiple charge configurations associated with each indirect neutral and charged excitons.
[42] A. Beckel, A. Kurzmann, M. Geller, A. Ludwig, A. D. Wieck, J. König, and A. Lorke, Europhys. Lett. **106**, 47002 (2014).
[43] M. Geller, B. Marquardt, A. Lorke, D. Reuter, and A. D. Wieck, Nanoscale Res. Lett. **5**, 829 (2010).
[44] R. J. Warburton, B. T. Miller, C. S. Dürr, C. Bödefeld, K. Karrai, J. P. Kotthaus, G. Medeiros-Ribeiro, P. M. Petroff, and S. Huant, Phys. Rev. B **58**, 16221 (1998).
[45] B. T. Miller, W. Hansen, S. Manus, R. J. Luyken, A. Lorke, J. P. Kotthaus, S. Huant, G. Medeiros-Ribeiro, and P. M. Petroff, Phys. Rev. B **56**, 6764 (1997).
[46] L. P. Kouwenhoven, D. G. Austing, and S. Tarucha, Rep. Prog. Phys. **64**, 701 (2001).
[47] S. Hameau, Y. Guldner, O. Verzelen, R. Ferreira, G. Bastard, J. Zeman, A. Lemaître, and J. M. Gérard, Phys. Rev. Lett. **83**, 4152 (1999).
[48] T. Ihn, *Semiconductor Nanostructures: Quantum states and electronic transport* (Oxford University Press Inc., New York, 2012).
[49] J. E. Rolon and S. E. Ulloa, Phys. Rev. B **82**, 115307 (2010).
[50] M. Ediger, G. Bester, A. Badolato, P. M. Petroff, K. Karrai, A. Zunger, and R. J. Warburton, Nat. Phys. **3**, 774 (2007).